AIP | The Journal of Chemical Physics

Perspective: Electrospray photoelectron spectroscopy: From multiply-charged anions to ultracold anions

Lai-Sheng Wang

Citation: The Journal of Chemical Physics **143**, 040901 (2015); doi: 10.1063/1.4927086
View online: http://dx.doi.org/10.1063/1.4927086
View Table of Contents: http://scitation.aip.org/content/aip/journal/jcp/143/4?ver=pdfcov
Published by the AIP Publishing

Perspective: Electrospray photoelectron spectroscopy: From multiply-charged anions to ultracold anions

Lai-Sheng Wang[a)]
Department of Chemistry, Brown University, Providence, Rhode Island 02912, USA

(Received 24 May 2015; accepted 25 June 2015; published online 22 July 2015)

Electrospray ionization (ESI) has become an essential tool in chemical physics and physical chemistry for the production of novel molecular ions from solution samples for a variety of spectroscopic experiments. ESI was used to produce free multiply-charged anions (MCAs) for photoelectron spectroscopy (PES) in the late 1990 s, allowing many interesting properties of this class of exotic species to be investigated. Free MCAs are characterized by strong intramolecular Coulomb repulsions, which create a repulsive Coulomb barrier (RCB) for electron emission. The RCB endows many fascinating properties to MCAs, giving rise to meta-stable anions with negative electron binding energies. Recent development in the PES of MCAs includes photoelectron imaging to examine the influence of the RCB on the electron emission dynamics, pump-probe experiments to examine electron tunneling through the RCB, and isomer-specific experiments by coupling PES with ion mobility for biological MCAs. The development of a cryogenically cooled Paul trap has led to much better resolved PE spectra for MCAs by creating vibrationally cold anions from the room temperature ESI source. Recent advances in coupling the cryogenic Paul trap with PE imaging have allowed high-resolution PE spectra to be obtained for singly charged anions produced by ESI. In particular, the observation of dipole-bound excited states has made it possible to conduct vibrational autodetachment spectroscopy and resonant PES, which yield much richer vibrational spectroscopic information for dipolar free radicals than traditional PES. © *2015 AIP Publishing LLC.* [http://dx.doi.org/10.1063/1.4927086]

I. INTRODUCTION

The first paper on electrospray by John Fenn in 1984 is titled "Electrospray Ion Source. Another Variation on the Free-Jet Theme."[1] In this prophetic article, Fenn envisioned three possible applications of the electrospray ionization (ESI) source. First and foremost, "this novel ion source may be useful for producing in vacuo a wide variety of cluster ions for examination by various spectroscopic techniques." Second is "the prospect of extending the applicability of mass spectrometric analysis to large organic molecules that are too complex, too fragile, or too nonvolatile for ionization by more conventional methods." Third, there exists "intriguing possibility to use this technique on probing the microscopic structure and properties of solutions." Indeed, the application of ESI in mass spectrometry of complex and nonvolatile molecules was immediately realized and has revolutionized mass spectrometric analyses of biological molecules.[2,3] However, its use as a novel ion source for spectroscopy took more than a decade to be realized, until it was first coupled with photoelectron spectroscopy (PES) in 1998 for the investigation of multiply-charged anions (MCAs).[4–6] Since then, ESI has been used widely as an ion source for various spectroscopic techniques,[7–31] just as Fenn envisioned. It has become an indispensible tool in chemical physics and physical chemistry in the production of interesting and novel ionic species from solution samples.

In this article, I provide a personal perspective on the application of ESI in photoelectron spectroscopy, starting from the initial motivation to study MCAs to more recent development, in particular, the coupling of the ESI source to a cryogenically cooled Paul trap that has made it possible to perform high-resolution PES. A number of reviews and perspectives on the PES of MCAs have appeared;[32–36] and this perspective focuses on more recent advances. The article is organized as follows. In Sec. II, the current configuration of the ESI-PES apparatus at Brown University, featuring a second-generation cryogenically cooled Paul trap and a state-of-the-art high-resolution PE imaging system, is described. Efforts in active cooling of molecular ions in cryogenic ion traps and its impact on spectroscopy will be mentioned. In Sections III–V, recent advances in PE imaging, pump-probe experiments, and isomer-specific experiments on MCAs will be described. Section VI presents high-resolution PES afforded by coupling the cryogenic Paul trap and PE imaging on singly charged anions from ESI. In Section VII, I discuss the observation of dipole-bound excited states in singly charged anions, which have dipolar neutral cores. The effects of cold anions on photodetachment spectroscopy via vibrational autodetachment from dipole-bound states (DBSs) and the potentials of resonant PES via the dipole-bound states are presented. The article is concluded with a brief summary and outlook for electrospray photoelectron spectroscopy.

II. EXPERIMENTAL METHODS

The first ESI-PES apparatus designed for the study of MCAs involved a home-built ESI source coupled to a room

[a)]E-mail: Lai-Sheng_Wang@brown.edu

temperature (RT) Paul trap for ion accumulation.[37] Ions were pulsed out of the ion trap into the extraction zone of a time-of-flight mass spectrometer at 10 Hz. The mass- and charge-selected ions were studied by a magnetic-bottle PES analyzer with an electron kinetic energy resolution of about 2% (ΔEk/Ek). The ion accumulation using the Paul trap and the high collecting efficiency of the magnetic-bottle PES analyzer were crucial, allowing many MCAs to be investigated.[4–6,32,33] The Kappes group successfully integrated an ESI source to a RT hexapole ion trap and a magnetic-bottle PES analyzer for the studies of MCAs.[38–40]

One of the limitations of the first ESI-PES apparatus was the lack of ion temperature control because the Paul trap was operated at room temperature. Molecular ions, in particular complex MCAs or weakly bounded anions, could carry substantial internal energies even at RT. Consequently, significant thermal broadening was observed, limiting the PES resolution and the accuracy of the measured electron binding energies. A second-generation ESI-PES apparatus was developed,[41] which featured a cryogenically cooled Paul trap. This advance not only allowed high-resolution PES data to be obtained by eliminating vibrational hot bands[42–45] but has also allowed temperature-dependent phenomena to be studied.[46–50] The first PES experiments performed using this newly built apparatus were the observation of C–H···O hydrogen bonding in long-chain alkane carboxylate anions at low temperatures[46] and the vibrationally resolved PE spectra of C_{60}^-, allowing the electron affinity (EA) of C_{60} to be measured with an accuracy of ±8 meV (2.683 ± 0.008 eV).[42] The largest anion that was completely vibrationally cooled using this instrument was the fullerene dimer oxide dianion, $[C_{60}OC_{60}]^{2-}$ with 121 atoms, for which vibrationally resolved PE spectra were obtained at low temperatures.[51] Even though the temperature of the anions was not known then in the cryogenic Paul trap, the effective cooling was demonstrated by the observation of H_2-tagged anions.[52] The second-generation ESI-PES apparatus staying at Pacific Northwest National Laboratory continues to yield interesting results.[53–55]

A. The third-generation ESI-PES apparatus

The second-generation ESI-PES apparatus is equipped with a magnetic-bottle PES analyzer, which has an electron energy resolution of about 2% (ΔEk/Ek), i.e., about 10–20 meV for low energy electrons under the best conditions.[41] Hence, the full benefits of actively cooling the anions cannot be fully capitalized due to the limited resolution of the magnetic-bottle PES analyzer. The third-generation ESI-PES apparatus developed recently at Brown University is shown schematically in Fig. 1, which couples a newly designed ESI and cryogenic Paul trap assembly with a high-resolution PE imaging system.[56] Both a Nd:YAG laser and a tunable dye laser (Δλ ~ 0.0015 nm, Sirah Cobra-Stretch with a frequency doubling unit) are equipped with this apparatus. Four major modifications were implemented in the new ESI-PES apparatus: (1) the ESI source with more compact ion optics; (2) the cryogenically cooled Paul trap with pulsed thermalization gas and a more powerful cryostat; (3) the replacement of the magnetic-bottle PES analyzer with a high-resolution co-linear PE imaging system; and (4) the improved vacuum system by replacing all diffusion pumps with turbomolecular pumps. The time-of-flight mass spectrometer is similar to the previous design,[37,41] with the exception of the ion detector, which is now placed in front of the co-linear PE imaging lens and can be moved out of the ion path during PE imaging experiments (Fig. 1). The capabilities and some initial results from this apparatus will be highlighted in Sections VI and VII. The high-resolution PE imaging system has been described in detail elsewhere.[56] The best resolution

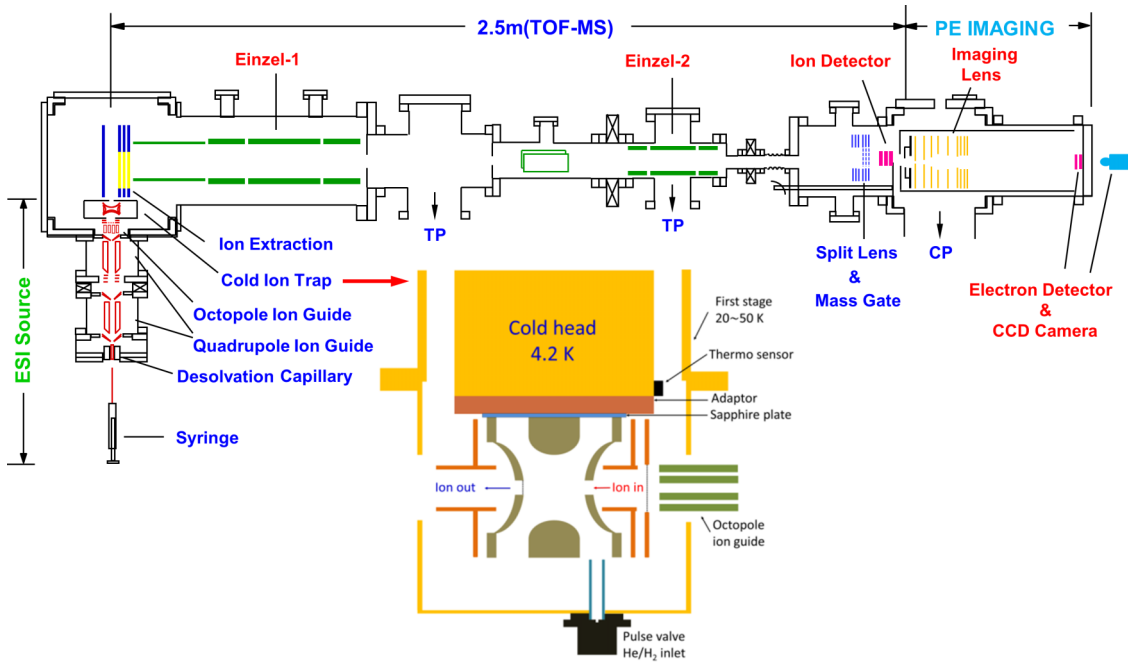

FIG. 1. Schematics of the current configuration of the third-generation ESI-PES apparatus at Brown University, featuring a cryogenic Paul trap and a high-resolution photoelectron imaging system (TP: turbomolecular pump; CP: cryopump).

achieved for near threshold electrons is 1.2 cm^{-1} (FWHM) from detachment of atomic anions and 2.8 cm^{-1} from Au_2^-, limited by rotational broadening.[57] Here, the new cryogenic Paul trap and the associated more compact ion optics are briefly discussed.

B. The cryogenic Paul trap

Controlling ion temperatures from ESI is challenging but extremely important in ion chemistry and spectroscopy. The linear 22-pole radio-frequency (RF) ion trap coupled with a closed-cycle helium refrigerator, developed by Gerlich,[58] has been adapted by a number of groups for ion spectroscopy.[11,59–65] The 22-pole trap has a rectangular-shaped trapping potential, which provides better ion cooling with minimal RF-heating. The linear design is also better suited for direct online laser excitation of the trapped ions. Following the Gerlich-type 22-pole design, a number of linear ion traps with lower pole numbers and other configurations have been designed with cryogenic cooling.[66–70] The lower pole numbers allow better on-axis focusing of trapped ions, more suitable for overlap with online laser excitations.[68] Our cryogenic ion trap involves a 3D Paul trap. Despite some initial skepticism, it has proven to perform quite well by completely eliminating vibrational hot bands in PES[41–45] and observation of temperature-dependent effects.[46–50] Recent high-resolution experiments showed that rotational temperatures can reach down to 20-35 K (see Section VII C), while the trap is operated at 4.4 K. The biggest advantage of the 3D Paul trap is its ease of operation and its suitability for extracting ions for subsequent time-of-flight mass analyses. A number of cryogenic Paul traps have been built recently to conduct spectroscopy on cold ions,[71–74] in particular, Johnson and co-workers have developed it into a powerful cryogenic ion spectroscopy technique via H_2 tagging.[28–30]

The current ESI Paul trap system at Brown University has been significantly improved over the first design.[41] The ion optics is much more compact without the 90° ion bender, as shown in Fig. 1. After the desolvation capillary, ions are transported by two sets of quadrupole ion guides and directed into the Paul trap (R. M. Jordan Co., Inc.) by an octopole ion guide. The ESI source and the first quadrupole ion guide can be tilted off axis via a flexible bellows, so that the neutral background gases from the high-pressure region would not reach the ion trap. However, it is found that the tilt is not necessary due to the efficient differential pumping. The ion trap is cooled by a customized two-stage closed-cycle helium refrigerator (Model SRDK from Janis Research Co., Inc.) that can cool down the ion trap assembly from RT to 4.4 K within about 1 h. The cooling gas, consisting of a mixture of 20% H_2 in He, is pulsed into the ion trap, according to Kamrath *et al.*[28] Ions are pulsed out of the Paul trap at a 10 Hz repetition rate into the time-of-flight mass spectrometer. The PE imaging chamber is pumped by a cryopump, while the chambers for the second octopole ion guide, the ion trap and extraction, and the time-of-flight mass analyzer are all pumped by turbomolecular pumps to eliminate any possibility of pump oils that would be undesirable for the operation of the cryogenic ion trap. The diffusion pumps used in the second-generation ESI-PES apparatus[41] were a significant problem, preventing operating the cryogenic Paul trap at the lowest possible temperature.

III. PHOTOELECTRON IMAGING OF MULTIPLY-CHARGED ANIONS: THE INFLUENCE OF THE REPULSIVE COULOMB BARRIER (RCB) ON THE PHOTOELECTRON EMISSION DYNAMICS

Although MCAs are ubiquitous in the condensed phases, isolated MCAs are usually not stable due to the strong intramolecular Coulomb repulsion and are difficult to form in the gas phase.[75–80] The coupling of ESI with PES allowed MCAs to be spectroscopically characterized for the first time.[4–6,32–40] When an electron is detached from a MCA, it experiences a short-range attraction by the nuclei and a long-range repulsion from the negatively charged residual ion, resulting in the so-called RCB (Fig. 2(a)). The RCB prevents slow photoelectrons from being emitted from MCAs, evidenced by a cutoff in PE spectra of all MCAs. The RCB provides dynamic stability to MCAs, allowing long-lived meta-stable MCAs with negative electron binding energies to be observed (Fig. 2(b)).[38,81–84]

The strong intramolecular Coulomb repulsion not only influences the energetics and stability of MCAs, but it is also expected to strongly influence the electron emission dynamics, which can be investigated using PE imaging by measuring the photoelectron angular distribution.[85–87] The first PE imaging on MCAs was done on a series of linear aliphatic dicarboxylate dianions [^-O_2C-$(CH_2)_n$-CO_2^-, n = 3–11],[88–90] which were expected to display strong anisotropy in the PE angular distribution. Because photoemission took place from one end of the MCAs, the outgoing electron was expected to be pushed to peak along the axis of the molecules. This anisotropy was observed as a parallel distribution along the laser polarization. Since the MCAs were not aligned, this observation suggested that there was a maximum detachment cross section when the linear dianions were aligned with the laser polarization. The anisotropy was observed to decrease with increasing chain length as the Coulomb repulsion decreases. At higher detachment photon energies, the anisotropy was also observed to decrease because of the increased kinetic energies of the outgoing electrons.[89] Even though photoelectron angular distributions are governed by partial wave interferences of the outgoing electron for neutral or singly charged anions,[86,87] the

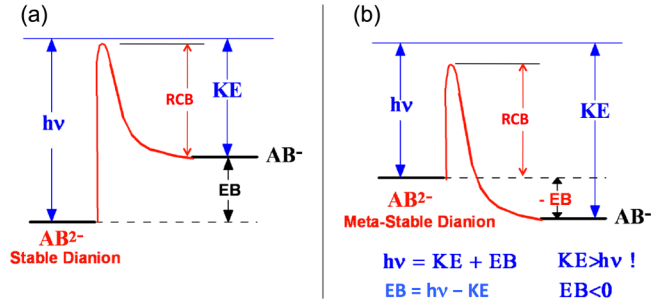

FIG. 2. Schematic potential energy curves showing the electron binding energy (BE) and the repulsive Coulomb barrier (RCB) in multiply-charged anions (using a doubly charged anion as an example): (a) for an electronically stable multiply-charged anion with a positive BE; (b) for a meta-stable multiply-charged anion with a negative BE because the electron kinetic energy (KE) is higher than the detachment photon energy (hν).

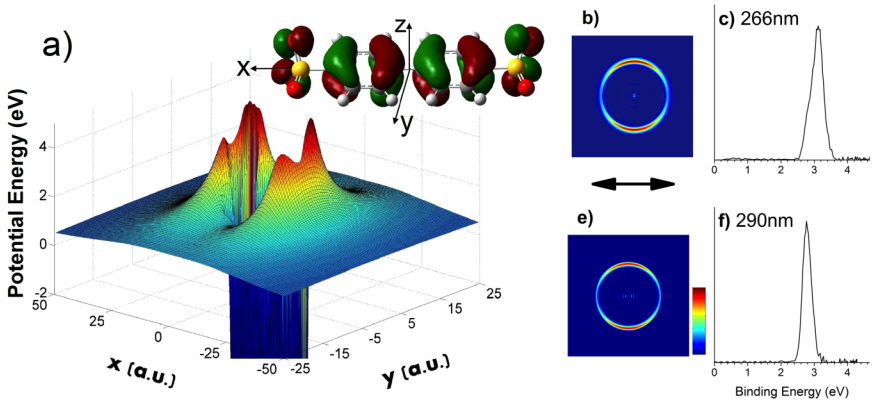

FIG. 3. (a) The calculated electrostatic potential for detaching an electron from the highest occupied molecular orbital (shown in the inset) of the diphenyl disulfonate dianion ($^{-}O_3S$-C_6H_4-C_6H_4-SO_3^{-}). (b) and (c) The photoelectron image and spectrum at 266 nm. (e) and (f) The photoelectron image and spectrum at 290 nm. The double arrow indicates the laser polarization.[92]

classical electrostatic effects dominate in MCAs and seem to have smeared out any quantum effects. Using the three isomers of benzene dicarboxylate dianions [*o*-, *m*-, *p*-$C_6H_4(CO_2)_2^{2-}$], we showed that the PE angular distributions were quite sensitive to the locations of the extra charges,[91] suggesting that PE imaging may allow structural information to be obtained for complex MCAs.

If electron detachment occurs from the central part of a linear doubly charged anion, one would expect a perpendicular electron emission pattern owing to the Coulomb repulsion from the two terminal negative charges. Indeed, this was observed in the PE imaging of the diphenyl disulfonate dianion[92] in which the highest occupied molecular orbital (HOMO) consists of the π system on the phenyl rings. Fig. 3(a) shows the HOMO and the structure of this dianion, as well as the calculated RCBs using the local approximation scheme.[93] Figs. 3(b) and 3(e) show the PE images at two different photon energies with strong perpendicular photoelectron distributions. In a control experiment, the PE angular distributions for a set of linear disulfonate dianions [$^{-}O_3S$-$(CH_2)_n$-SO_3^{-}, n = 1–3] were observed to exhibit parallel distributions because electron emission was from the $-SO_3^{-}$ end groups, similar to the linear dicarboxylate cases mentioned above. As shown below, Verlet and co-workers have also observed perpendicular PE angular distributions for several dianions with similar structures and charge carriers.[94–96]

IV. PUMP-PROBE EXPERIMENTS: PROBING ELECTRON TUNNELING THROUGH THE REPULSIVE COULOMB BARRIER AND EXCITED STATE DYNAMICS

Near the top of the RCB (Fig. 2), electron tunneling can occur, and it was shown that such tunneling can be approximately described using the nuclear tunneling model for α-decay.[82,97] The lifetimes of meta-stable MCAs are determined by the rate of electron tunneling.[98,99] The Kappes group has investigated electron tunneling in several meta-stable MCAs using mass spectrometry and photodetachment.[84,100–102] MCAs can be pumped to an excited state, from which fast electron tunneling can occur. Such resonant tunneling was first observed in the copper phthalocyanine tetrasulfonate tetra-anion.[83] The Kappes group used ultrafast pump-probe experiments to probe the dynamics of the excited states in several phthalocyanine MCAs and observed both resonant tunneling and internal conversion.[103,104] In a recent PES experiment on the bisdisulizole tetra-anion ($BDSZ^{4-}$), an intense constant kinetic energy peak was observed over a large range of photodetachment energies.[105] The same kinetic energy at different detachment photon energies suggested a common resonant tunneling state within the RCB, i.e., the tetra-anion absorbed a detachment photon at different energies but relaxed to the same lower excited state (assumed to be the S_1 lowest excited state), from which resonant tunneling occurred. A tunneling lifetime was estimated to be ~450 fs using a pump-probe experiment. Similar resonant tunneling was observed in a series of triply charged ion-pairs of $BDSZ^{4-}$ with alkali ions [M^{+} ($BDSZ^{4-}$)] and the tunneling lifetimes were found to be dependent on the alkali ions.[106]

Verlet and co-workers have recently coupled pump-probe experiments with PE imaging to probe the dynamics of MCAs and the effects of the RCB.[94–96,107,108] In an experiment on the deprotonated fluorescein dianion, they pumped the dianion to its S_1 excited state within the RCB and observed strong resonant tunneling.[107] They observed that the electron kinetic energies from the resonant tunneling and the tunneling lifetimes are constant when the pump laser was tuned to different vibronic levels of the S_1 state. These observations were explained using an adiabatic tunneling model, i.e., the internal energies in the S_1 excited state were preserved during electron tunneling through the RCB. This model should apply when electron tunneling is fast, relative to vibrational relaxation. On the other hand, if the tunneling lifetime is long in the nascent excited state relative to internal conversion or vibrational relaxation, one expects that tunneling would occur from the lowest or a lower excited state in the MCA following relaxation from the initial excitation.

In the PE imaging experiments of the linear dicarboxylates and disulfonate dianions discussed in Section III above, the MCAs were not aligned. One would expect much stronger anisotropy if aligned samples were possible. Verlet and co-workers have been able to achieve such alignment using pump-probe experiments of two doubly charged dye molecules, pyrromethene 556 (PM^{2-}) and doubly deprotonated indigo carmine.[36,94–96] Both dianions consist of a central aromatic system with two terminal sulfonate groups and a π HOMO on the aromatic system, very similar to the diphenyl disulfonate dianion shown in Fig. 3(a).[92] PE images using single photon detachment also revealed perpendicular angular distributions because the anisotropy of the RCB is similar to that of Fig. 3(a). However, both dianions are highly photoactive with long-lived S_1 excited states within the RCB. The transition

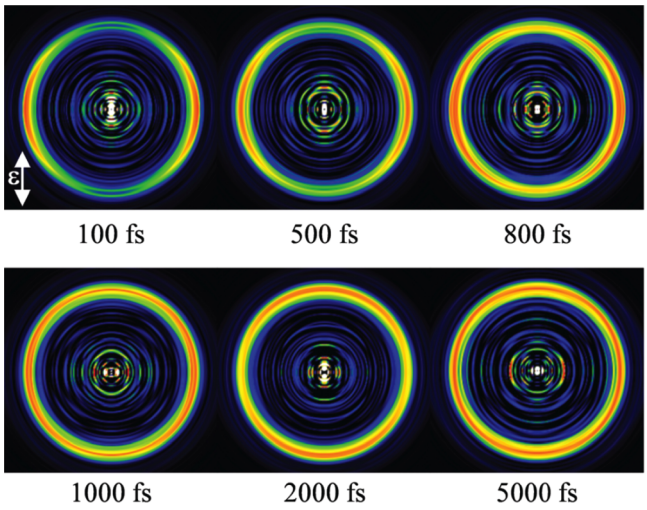

FIG. 4. Time-resolved photoelectron images by exciting the pyrromethene-556 dianion to its S_1 excited state with a 2.43 eV pump pulse followed by a 1.55 eV probe pulse at different delay times. The double arrow indicates the laser polarization. Reprinted with permission from Horke *et al.*, J. Phys. Chem. Lett. **3**, 834 (2012). Copyright 2012 American Chemical Society.

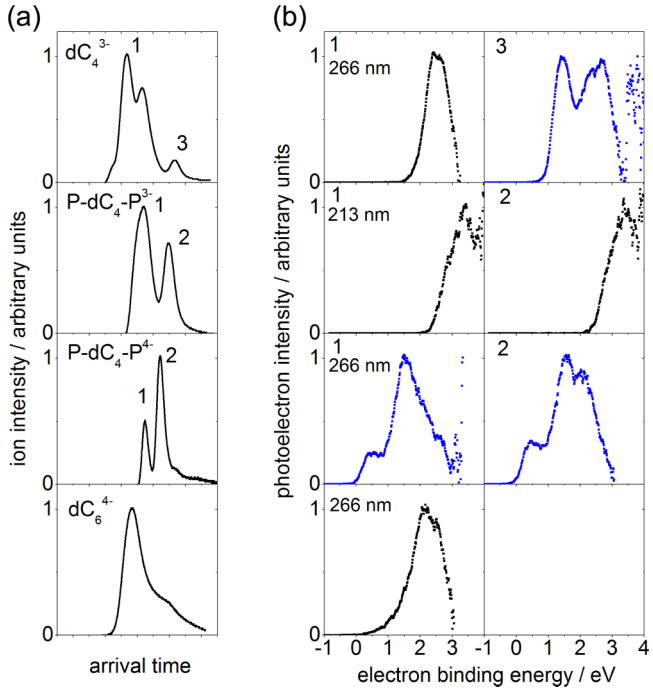

FIG. 5. The ion mobility arrival times (a) for four DNA oligonucleotide MCAs and the isomer-selected photoelectron spectra (b). See Ref. 111 for the structures of the oligonucleotides. Reprinted with permission from Vonderach *et al.*, J. Am. Chem. Soc. **134**, 7830 (2012). Copyright 2012 American Chemical Society.

dipole to the S_1 state is along the molecular axis defined by the two sulfonate groups. Hence, excitation to the S_1 state prepares an aligned sample along the laser polarization direction. A probe laser that detaches an electron from the S_1 state can probe the dynamics of the S_1 state, as shown in Fig. 4. At short delay times, a much stronger perpendicular angular distribution is observed because of the aligned S_1 state along the laser polarization. As the probe delay is increased, the anisotropy is decreased as a result of molecular rotation. In fact, at a delay time of 2 ps, a parallel angular distribution is observed, suggesting that the PM^{2-} dianions initially prepared in the S_1 state have undergone a 90° rotation. At long delay times, the angular distribution is isotropic because of the rotational dephasing. For short-lived excited states, one would expect that resonant tunneling or internal conversion may compete with the rotational dephasing, resulting in much more complicated angular distributions.

V. ISOMER-SELECTIVE PHOTOELECTRON SPECTROSCOPY OF MULTIPLY-CHARGED BIOMOLECULES

The most important application of ESI is in the mass spectrometric analyses of biomolecules, which are often in the form of multiply-charged cations or anions.[2,3] PES can be a valuable technique to probe the electronic structure and stability of negatively charged biomolecules.[109] However, many gaseous biomolecules exist as a mixture of different isomers, which have different structures, but similar thermodynamic stability. The presence of close-lying multiple isomers posed a major challenge to the application of PES to biomolecules. Ion mobility involves sending a mass-selected ion packet through a collision cell. Ions with different shapes or cross sections have different diffusion times in the collision cell and can be separated spatially and temporally. Ion mobility has become a powerful technique in biological mass spectrometry for structural determination. Isomer-selective PES using ion mobility was demonstrated for small carbon clusters in the size range of the linear-to-cyclic structural transition.[110]

Recently, the Kappes group has developed a novel instrument coupling ion mobility mass spectrometry with PES and obtained isomer-selective PES for MCAs of biomolecules.[111–113] Fig. 5(a) shows the ion mobility separation of four DNA oligonucleotide MCAs.[113] The corresponding PE spectra for the different isomers are shown in Fig. 5(b). Clearly, different isomers for the same MCA gave different PE spectra. The PES resolution here was limited because of both the complexity of the MCAs and more importantly their internal energies. These experiments were performed at RT and the large MCAs were expected to carry significant thermal energies to cause vibrational broadening. Hence, cooling of the isomer-selected MCAs following ion mobility separation would enhance the spectral resolution.

VI. HIGH-RESOLUTION PHOTOELECTRON IMAGING AND SPECTROSCOPY OF COLD ANIONS FROM ELECTROSPRAY

The coupling of the cryogenic Paul trap with an ESI source in the second-generation ESI-PES apparatus has significantly improved the quality of the PE spectra of MCAs, as well as that of singly charged anions.[41–55] Issendorff and coworkers have also coupled a cryogenic 12-pole linear ion trap with a magnetic-bottle PES analyzer for the study of atomic clusters.[114] The moderate resolution of the magnetic-bottle analyzer is sufficient for MCAs, for which no slow electrons are possible due to the RCB. However, for singly

charged anions, the cryogenic Paul trap offers an opportunity to conduct high-resolution PES using PE imaging. In contrast to the magnetic-bottle analyzer, the imaging method allows very slow electrons to be detected, including zero eV electrons. The energy resolution for slow electrons can be extremely high in PE imaging. The Neumark group has exploited this property and developed slow electron velocity-map imaging (SEVI) into a new type of high-resolution PES for anions,[115–117] which yields comparable resolution as ZEKE, but is much more advantageous in its implementation and operation. In SEVI, a series of PE images are obtained using a tunable detachment laser. Then, the high-resolution parts of these spectra (i.e., the slow electrons) are cut out and stitched together to form a high-resolution SEVI spectrum.[117] We have found that it is often valuable to present the full set of PE images and spectra taken at different detachment energies, because there may be interesting energy-dependent spectral features, such as resonant phenomena or near threshold enhancement.

A. High-resolution PE imaging of the cold fullerene C_{60}^- anion

Fig. 6 shows a comparison of the PE spectra of C_{60}^- using the first- and second-generation ESI-PES apparatuses,[42,118] and the new PE imaging data on the third-generation apparatus.[119] Qualitative improvement was observed using the second-generation ESI-PES apparatus by cooling the C_{60}^- anion to 70 K, evidenced by the elimination of the hot bands (red curve in Fig. 6(a)), but the spectrum was limited by the resolution of the magnetic-bottle analyzer. An extensive set of PE images were taken for C_{60}^- on the third-generation apparatus at different detachment wavelengths.[119] Figs. 6(b)-6(d) reproduce the PE images and spectra at three photon energies. In addition to the interesting angular distributions, significant photon-energy dependent effects were observed. For example, the 0-0 transition is no longer the strongest peak at the lower photon energies (Figs. 6(c) and 6(d)). A total of sixteen vibrational peaks were resolved for the ground electronic state of C_{60}, yielding fourteen fundamental vibrational frequencies, many of which were obtained for the first time for gaseous C_{60}. Furthermore, the EA of C_{60} was accurately measured as 2.6835(6) eV, resolving some major uncertainly in the literature.[120] Recently, the Neumark group has also coupled a cryogenic octopole ion trap with PE imaging and obtained high resolution PES data for cold atomic clusters from a laser vaporization source or supersonic ion beam source for molecular anions.[121–124]

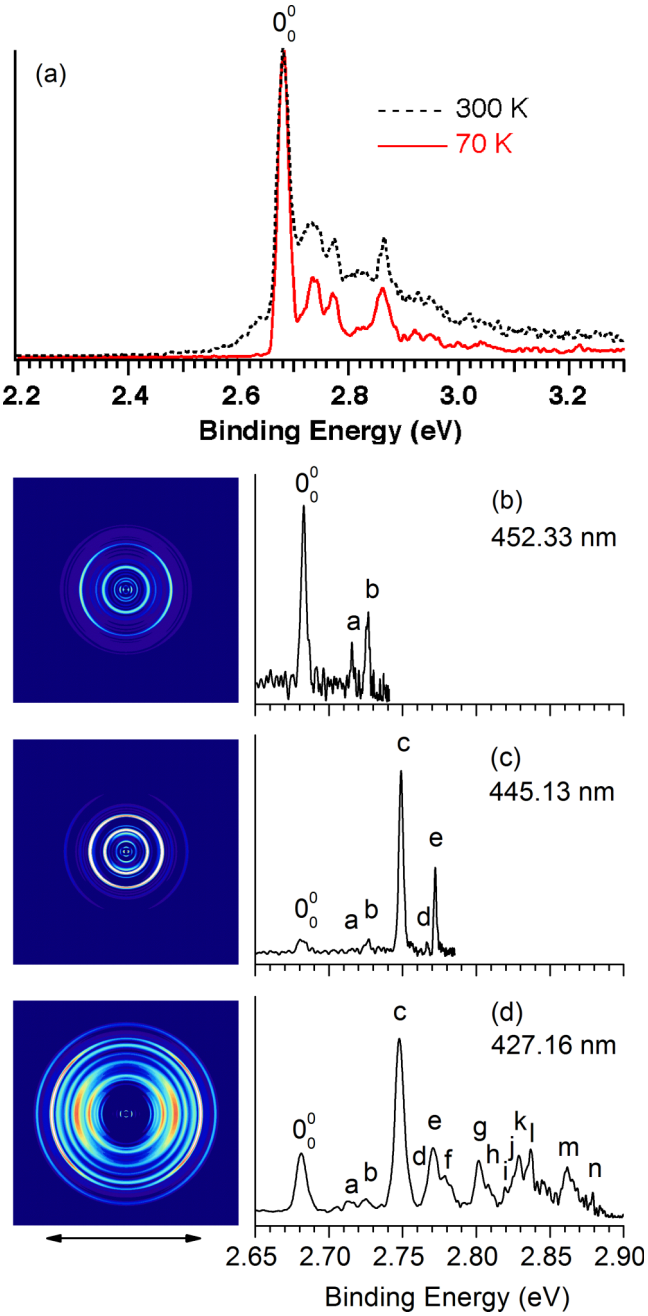

FIG. 6. Comparison of the photoelectron spectra of C_{60}^- from the magnetic-bottle electron analyzer on the first- and second-generation ESI-PES apparatuses (a) to that of the third-generation apparatus coupling a cryogenic Paul trap and high-resolution photoelectron imaging (Figure 1) at three detachment wavelengths (b)–(d). The double arrow indicates the laser polarization.[119]

B. Vibrational state-selective resonant two-photon high-resolution PE images of AuS^-

Even though the ESI source was considered to be a soft ionization method by transporting solution ionic species into the gas phase, ion-molecule reactions or collision-induced dissociations can occur during electrospray, most likely in the high pressure region right after the desolvation capillary and in front of the first skimmer (Fig. 1). For example, in an experiment aimed at producing Au-thiolate clusters,[125] simple anions, such as Au^-, AuH_2^-,[126] and AuS^-,[127] were observed and they must come from ion molecule reactions or collision-induced dissociations. The AuS^- anion was previously produced using a laser vaporization cluster source and its electronic structure was investigated by the magnetic-bottle PES apparatus and *ab initio* calculations.[128] The production of the AuS^- anion from the ESI source afforded an opportunity to obtain high-resolution PE spectra of cold AuS^- on the third-generation ESI-PES apparatus.

It was during the search for dipole-bound states in AuS^- (see below) that a valence electronic excited state was observed for AuS^-, 0.1089 eV below the detachment threshold ($C^3\Sigma^-$

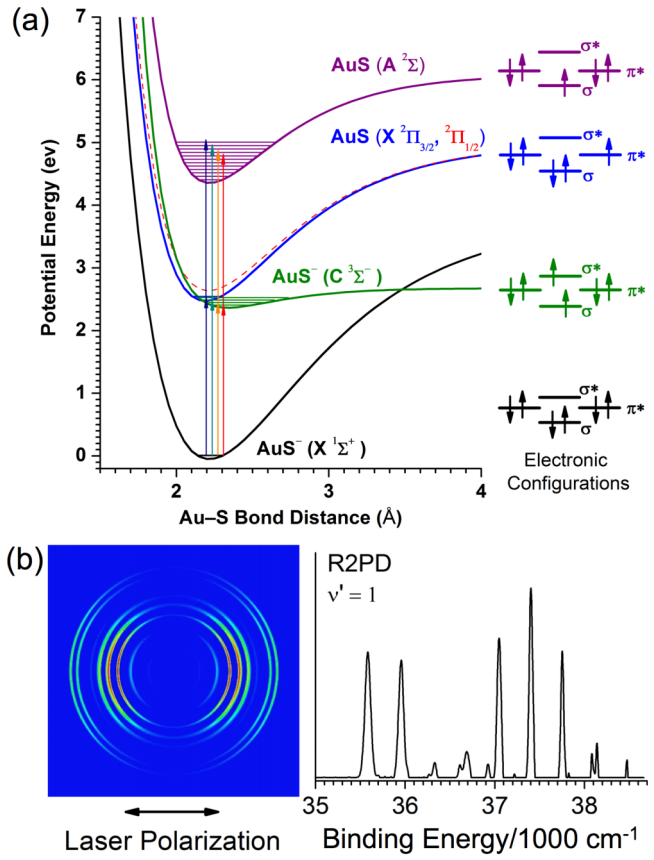

FIG. 7. (a) Schematic potential energy curves showing the ground state ($X^1\Sigma^+$) and an excited state ($C^3\Sigma^-$) of AuS^- and the ground state ($X^2\Pi$) and the first excited state ($A^2\Sigma$) of AuS and their electron configurations. (b) The vibrational-selective photoelectron image and spectrum of AuS^- via the $v' = 1$ vibrational level of the $C^3\Sigma^-$ electronic state of AuS^- to the $A^2\Sigma$ final state of AuS. The double arrow below the image indicates the laser polarizations.[127]

in Fig. 7(a)). Eight vibrational levels ($v' = 0$–7) were observed for the $^3\Sigma^-$ excited state using resonant two-photon detachment spectroscopy.[127] Four long-lived levels ($v' = 0$–3) were bound-states below the detachment threshold, and four short-lived levels ($v' = 4$–7) were found to be above the detachment threshold and underwent autodetachment. The four bound vibrational levels allowed vibrational state-selective PE images to be obtained by resonant two-photon detachment via the $^3\Sigma^-$ excited state. Fig. 7(b) shows a PE image from the $v' = 1$ level of the $^3\Sigma^-$ intermediate state to the $^2\Sigma$ final state of neutral AuS, with an unusual Franck-Condon envelope. PE images were obtained from all the four bound levels ($v' = 0$–3) of the $^3\Sigma^-$ state, each with a very different Franck-Condon envelope, reflecting the symmetry of the initial vibrational wavefunctions in the $^3\Sigma^-$ state. In fact, some vibrational levels were resolved to be doublet, due to spin-spin coupling in the $^3\Sigma^-$ state. The *p*-wave angular distribution was consistent with the nature of the σ* electron that was detached by the second photon (see electron configurations in Figure 7(a)). Excitation to the $^3\Sigma^-$ excited state of AuS^- involved a spin-forbidden transition from the $^1\Sigma^+$ ground state, in agreement with the long lifetime of this state. Interestingly, three low-lying excited states were also predicted to exist for AuS^- below the $^3\Sigma^-$ state,[127] which can be accessed by $1 + 1'$ or $1 + 1$ resonant two-photon detachment.

VII. RESONANT PHOTOELECTRON SPECTROSCOPY VIA DIPOLE-BOUND EXCITED STATES

A. PES of phenoxide at room temperature and observation of dipole-bound states

High-resolution PE images for singly charged anions from ESI were first attempted on the phenoxide anion using the RT Paul trap on the first-generation ESI-PES apparatus.[37] The phenoxide anions could be produced readily from ESI of a basic solution of phenol, but the PES results were a complete surprise, as shown in Fig. 8. The spectrum displayed in Fig. 8(b) was obtained at 409.37 nm with the resolution of a single vibrational progression (defined by peaks *b*, *c*, *d* . . .) and a vibrational hot band transition (defined by peak *a*). This spectrum was consistent with a previous PES study using a hemispherical electron analyzer.[129] As the detachment photon energy was decreased, the spectral resolution was improved (Fig. 8(c)), but the peak width was not significantly reduced because of ro-vibrational broadening. This could be seen clearly for the spectrum at 546.43 nm, which was near the detachment threshold. But the 0-0 transition defined by peak *b* was much broader than the instrumental resolution. Surprisingly, sharp peaks appeared in the lower photon energy spectra (Fig. 8(c)). Most strikingly, the spectrum at 538.18 nm consisted mainly of one very strong and sharp peak with a width close to the instrumental resolution. Furthermore, the sharp peaks seemed to exhibit constant kinetic energies, as seen in Fig. 8(d). The constant kinetic energies and the intense nature of the sharp peaks suggested that they must be due to excitation to some autodetaching resonant states.

Further experimentation with different anions showed that such sharp features existed only for anions with a dipolar neutral core, strongly suggesting that they came from excited DBSs. DBS was predicted to exist for neutral molecules with sufficiently large dipole moments (>2.5D)[130–133] and had been observed,[134–138] usually with very low binding energies. Excited DBSs near the detachment thresholds of anions were observed by Brauman and co-workers in photodetachment cross sections.[139–142] The excited DBSs in anions with neutral dipolar cores are analogous to Rydberg states in neutral molecules. Because the binding energies of DBSs were on the order of a few to few tens of wavenumbers, vibrational or rotational autodetachment can occur, resulting in resonances in the detachment cross sections. Lineberger and co-workers had performed high-resolution autodetachment spectroscopy via DBS.[143–148] The phenoxy radical has a sufficiently large dipole moment (~4 D) (see inset of Fig. 8(b)) and it was plausible that phenoxide could have excited DBS near its detachment threshold. The wave function of the DBS was calculated and shown in Fig. 8(a). However, one puzzling issue was why the sharp peaks observed in Fig. 8(c) seemed to have no wavelength dependence. In the meantime, SEVI spectra had been reported for phenoxide produced from a supersonic ion beam.[149] The moderate cooling of phenoxide in this study appeared to be critical, even though vibrational hot bands were still observable. Most importantly, no similar sharp peaks were observed in the reported SEVI spectra. Clearly, the observation of DBS resonances in the PE spectra of RT phenoxide was due to the temperature effects: the internal energies in the hot

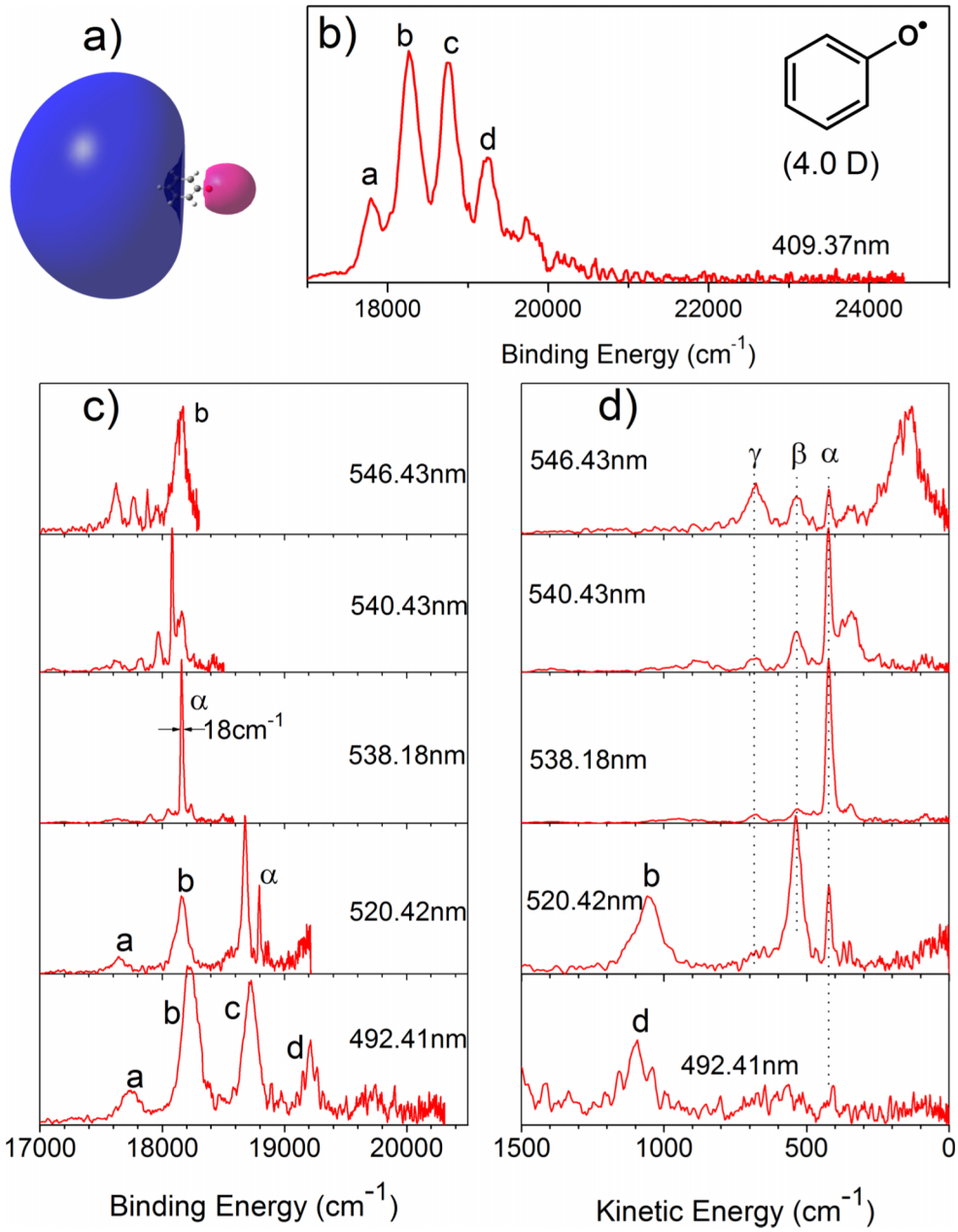

FIG. 8. Photoelectron spectra of phenoxide ($C_6H_4O^-$) at room temperature. (a) The wave function of the dipole-bound excited state of phenoxide. (b) The photoelectron spectrum at 409.37 nm. (c) Photon energy dependent photoelectron spectra from 492.41 nm to 536.43 nm. (d) The same data plotted in kinetic energy scale, highlighting the constant kinetic energy nature of the unexpected sharp peaks (α, β, γ). The inset in (b) shows the structure of the phenoxy radical and its dipole moment.

anions made it possible for resonant excitations to the DBS at much broader photon energy ranges.

B. Resonant PE imaging and spectroscopy of cold phenoxide via dipole-bound states

The PE images and spectra of cryogenically cooled phenoxide done on the third-generation ESI-PES apparatus are shown in Fig. 9 (left).[150] These spectra were hugely improved in comparison with the RT data in Fig. 8(c). In fact, the near threshold 0-0 transition at 549.43 nm (Fig. 9(a)) was partially rotationally resolved, as seen from the fine features in the expanded spectrum in the inset. The constant kinetic energy sharp peaks were no longer observed. In comparison to the SEVI spectrum taken with the supersonic ion beam,[149] vibrational hot bands were completely eliminated in the spectra presented in Fig. 9. Hence, in addition to the main vibrational progression due to the ν_{11} mode, a number of weak peaks and combinational vibrational levels with weak Franck-Condon factors were resolved and assigned, i.e., the ν_9, ν_{10}, and ν_{18} modes.

Apparently, the cold anions without a large amount of rovibrational energies made it more difficult to observe the DBS. To search for the DBS, we scanned the dye laser above the detachment threshold by monitoring the total electron yield and found eight autodetaching vibrational levels, as shown schematically in Fig. 10, where the vibrational levels of the neutral phenoxy are also shown. We were also able to observe

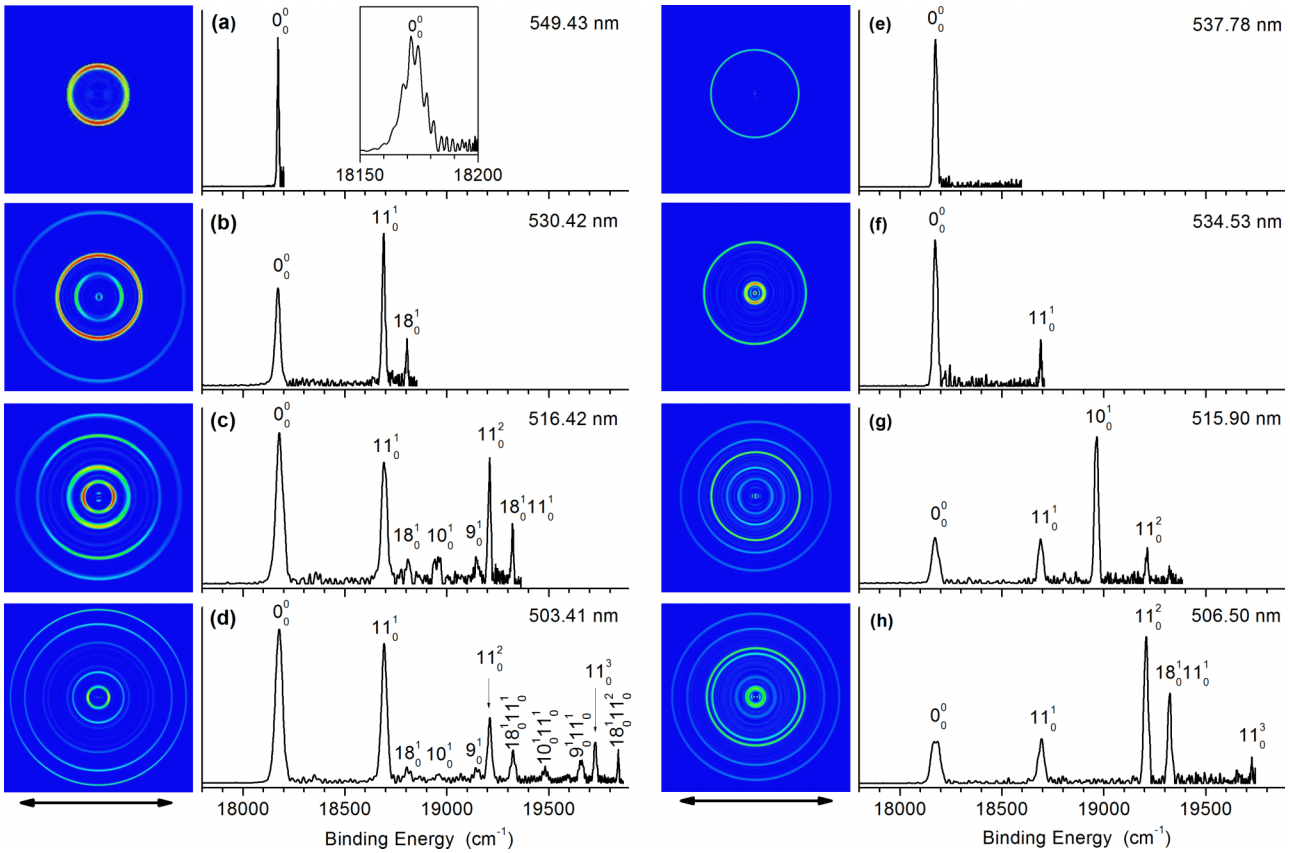

FIG. 9. Comparison of the non-resonant photoelectron images and spectra of phenoxide ($C_6H_5O^-$) (left) to resonant photoelectron images and spectra via dipole-bound excited states. The double arrows below the images indicate the laser polarization.[150]

the DBS ground state by resonant two-photon detachment. The binding energy of the DBS was measured to be 97 cm^{-1} relative to the detachment threshold at 18 173 cm^{-1}, i.e., the EA of phenoxy. By tuning the detachment laser to each vibrational level of the DBS, we obtained resonantly enhanced PE spectra, which consisted of both direct detachment and autodetachment. Because the electron in the DBS is so weakly bound and outside the neutral core (see Fig. 8(a)), the structure of the anion in the DBS and that of the neutral phenoxy is the same. In fact, a detachment spectrum was obtained by scanning the laser near the ν_{11} vibrational levels and the ν_{11} frequency measured for the DBS was found to be identical to that of the neutral phenoxy, as resolved in the PE spectra. Thus, there is a propensity rule of $\Delta v = -1$ for the autodetachment,[151] first derived for autoionization of Rydberg states of H_2.[152] The allowed and observed autodetachment channels are indicated in Fig. 10.

The right hand side of Fig. 9 shows four resonantly enhanced PE images and spectra. The spectrum in Fig. 9(e) corresponded to the excitation of the first overtone of the ν_{11} mode ($11'_0{}^1$), leading to a very intense 0-0 peak. The angular distributions from the autodetachment-enhanced peak and that of the direct detachment are different, as can be seen in the PE images of Figs. 9(a) and 9(e). The direct detachment transition gave a somewhat perpendicular distribution, whereas the autodetachment transition gave an isotropic distribution. The spectrum in Fig. 9(f) corresponded to the excitation of the first overtone of the ν_{18} mode ($18'_0{}^1$), which also led to an enhanced 0-0 transition and the highly non-Franck-Condon PE spectrum. The spectrum in Fig. 9(g) corresponded to excitation to a combinational level of the DBS ($10'_0{}^1 11'_0{}^1$) (Fig. 10). Coupling of one quantum of the ν_{11} mode to the outgoing electron led to the significantly enhanced 10_0^1 peak, which had a very weak Franck-Condon factor in the non-resonant PE spectra (Figs. 9(c) and 9(d)). The spectrum in Fig. 9(h) involved excitation to the $18'_0{}^1 11'_0{}^2$ combinational level of the DBS (Fig. 10). Hence, coupling of one ν_{18} quantum to the outgoing electron led to the significantly enhanced 11_0^2 peak, and coupling of one ν_{11} quantum led to the enhanced $18_0^1 11_0^1$ combinational peak in the PE spectrum. These represented the first resonantly enhanced PE spectra via the DBS and were valuable to obtain vibrational frequencies of the neutral radicals for those modes, which have weak Franck-Condon factors.

C. Photodetachment spectroscopy of cold anions via autodetachment from vibrational levels of excited dipole-bound states

The cryogenic Paul trap coupled with ESI provides further opportunities to perform vibrational autodetachment spectroscopy via DBS by monitoring the total electron emission signals as a function of the detachment laser wavelength, near and above the detachment threshold. Because the structures of the dipole-bound anions are practically identical to that of the neutral radical core, autodetachment spectroscopy can be used

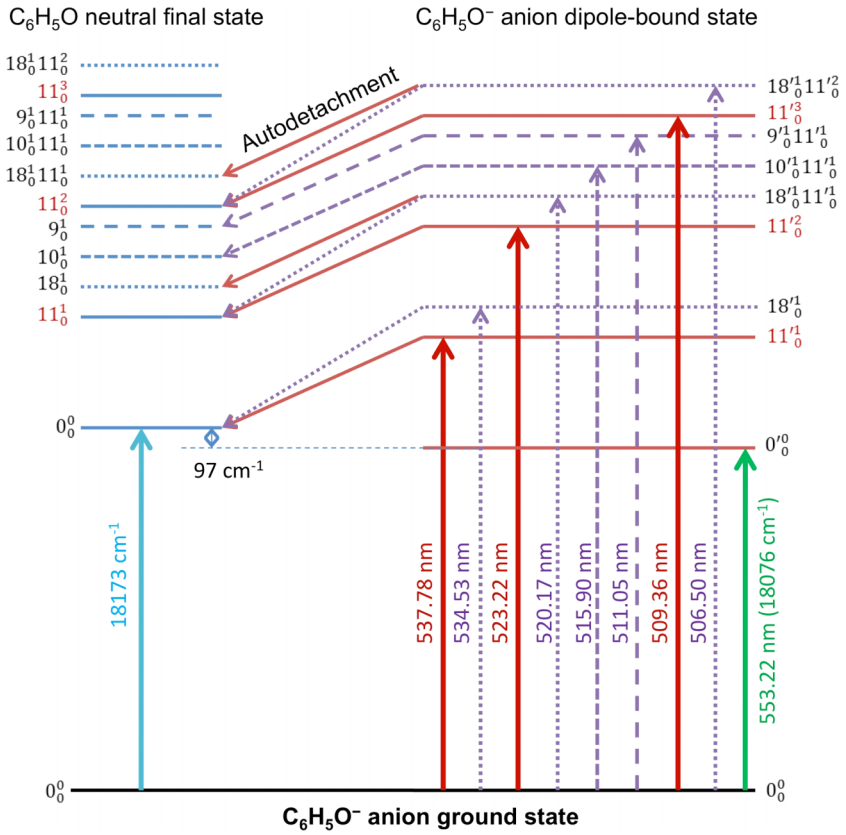

FIG. 10. The schematic energy level diagram for the direct detachment to the vibrational levels of phenoxy (left) and the vibrational levels of the excited dipole-bound state of phenoxide (right). The vertical arrows represent the resonant excitations with the corresponding wavelengths. Autodetachment transitions from the vibrational levels of the dipole-bound state to the vibrational levels of neutral phenoxy are indicated. The final-state vibrational levels of the autodetachment would be enhanced in resonant PE spectra, resulting in highly non-Franck-Condon distributions.[150]

to probe vibrational properties of interesting neutral radicals using optical excitation. Lineberger and co-workers used autodetachment to perform rotational spectroscopy using a high-resolution laser,[143–148] but with narrow wavelength ranges. Furthermore, the limited cooling capacity often yielded quite congested autodetachment spectra even for relatively simple anions.

The first systematic vibrational autodetachment spectrum obtained using the third-generation ESI-PES apparatus was on the deprotonated uracil anion ([U-H]$^-$) (see inset of Fig. 11(b) for its structure).[153] The [U-H]• radical has a calculated dipole moment of ~3.2 D, sufficient to bind an electron to give rise to an excited DBS for the anion. The wave function of the DBS excited state of [U-H]$^-$ is shown in Fig. 11(a) as an inset. The autodetachment spectrum shown in Fig. 11 covered an energy range of 1850 cm^{-1} starting from just below the detachment threshold at 28 076 cm^{-1} (indicated by the arrow). A total of 46 autodetachment vibrational peaks were observed. The very weak peak below the threshold at 27 930 cm^{-1} came from resonant two-photon detachment and represented the ground state of the DBS, giving rise to a binding energy of 146 cm^{-1}. A clear step was observed at the detachment threshold (see the arrow) and the continuous baseline above threshold represented the total electron yield of non-resonant detachment. Thus, each above-threshold autodetachment peak should have a Fano line shape,[154,155] which was observed more clearly for peak 5 near the baseline (Fig. 11). Many of the observed peaks corresponded to combinational vibrational levels of the DBS. Twenty-one fundamental vibrational frequencies were obtained out of a total of 27 for the [U-H]• radical, in particular, all the low-frequency modes including symmetry-forbidden out-of-plane modes were observed.[153]

More interestingly, rotational profiles were resolved for the vibrational resonances and allowed the rotational temperature of the anions in the cryogenic Paul trap to be characterized quantitatively. Fig. 11(b) presents a comparison of the simulated rotational profile for peaks 8 and 9, using the PGOPHER program.[156] Peak 8 (ν_{16}) corresponded to a *c*-type transition and peak 9 (ν_{24}) was a *b*-type transition. The simulation yielded a rotational temperature of T_{rot} = 35 K, while the cryogenic trap was operated at 4.4 K measured off the trap surface using a silicon diode temperature sensor. More recent experiments on the deprotonated thymine anion gave rise to a similar rotational temperature,[157] whereas a slightly lower rotational temperature was observed for the smaller acetate anion (~20-35 K),[158] which was the lowest rotational temperature achieved thus far in the cryogenic Paul trap. The discrepancy between the nominal trap temperature (4.4 K) and the achieved ion temperature is most likely due to the RF-heating. Surprisingly, the achievable temperature in the Paul trap is not significantly inferior in comparison to the 22-pole trap (T_{rot} ~ 10-20 K),[62,63] which is supposed to have less RF-heating. It is interesting to note that ion traps are more effective at vibrational cooling and less effective at rotational cooling due to RF-heating, in contrast to the cooling effects in supersonic molecular beams, where rotational cooling is much more effective than vibrational cooling.

By tuning the detachment laser to the autodetachment peaks, resonant-enhanced PE images and spectra can be obtained, like those shown in Figs. 9(e)-9(h). Such highly non-Franck-Condon resonant PE spectra are not only valuable

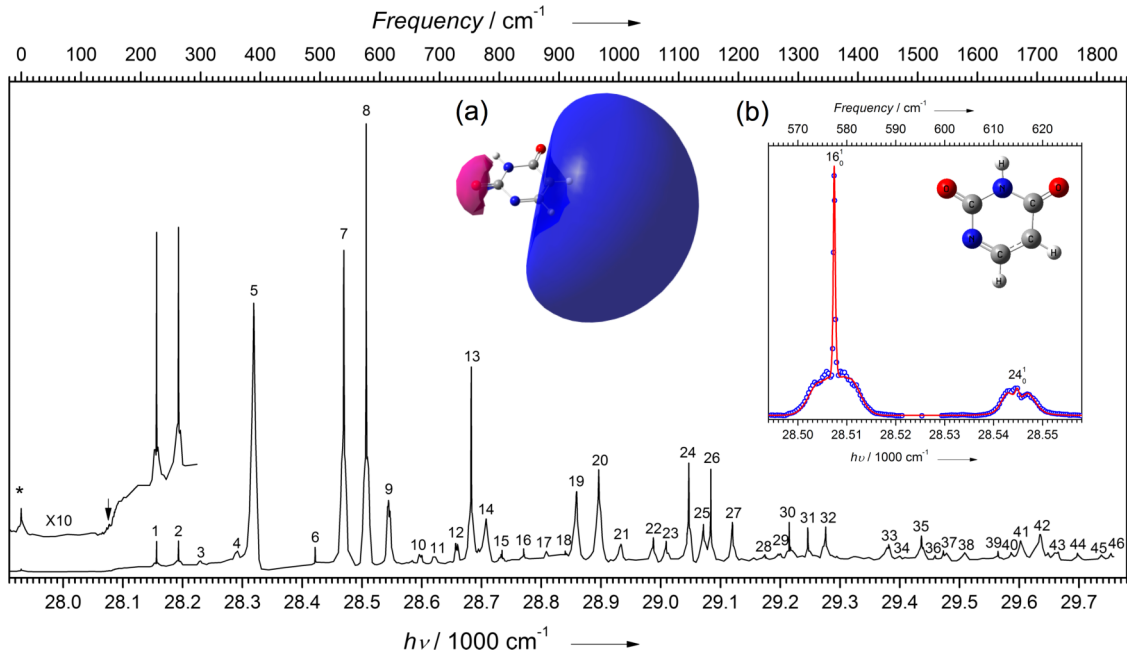

FIG. 11. Photodetachment spectroscopy via the dipole-bound state of the deprotonated uracil anion. (a) The calculated wave function of the dipole-bound state. (b) Comparison of the simulated rotational profiles for peaks 8 and 9. A rotational temperature of $T_{rot} = 35$ K was obtained. The inset in (b) shows the structure of the deprotonated uracil anion (red: O; blue: N; dark grey: C; light grey: H).[153]

to provide accurate measurements of vibrational frequencies for those modes with weak Franck-Condon factors, they are also important in the assignments of the observed vibrational levels of the DBS. In fact, the assignments of the 46 observed autodetachment resonances for $[U\text{-}H]^-$ were done by measuring the resonant PE spectra in conjunction with calculated frequencies. The potentials of resonant PES via DBS have been illustrated in a number of recent studies.[157–159] The resonant PES led to the definitive determination of the 0-0 detachment transition in the acetate anion, allowing the EA of the acetyloxyl radical to be accurately and unambiguously measured.[158] Autodetachment spectroscopy and resonant PE images and spectra for the deprotonated thymine and the 2-hydroxyphenoxide anions have also been reported recently,[157,159] allowing the measurements of the vibrational frequencies of the corresponding neutral radicals and further demonstrating the potentials of resonant PES via DBS as a new technique for vibrational spectroscopy of novel radical species.

VIII. CONCLUDING REMARKS

Since the first coupling of ESI with photoelectron spectroscopy, the application of ESI has blossomed in a myriad of new spectroscopic techniques. It has become an indispensible tool in chemical physics for the spectroscopic investigation of solution-based ionic species, in particular, biological molecules and reaction intermediates. The combination of ESI with cryogenic ion trap technology has played a major role in the expansion of ESI in spectroscopic applications, which has largely fulfilled Fenn's original vision of ESI as "Another Variation on the Free-Jet Theme."[1] As a matter of fact, vibrational cooling works spectacularly well in cryogenic ion traps, even though the rotational cooling is slightly inferior in comparison to free-jet expansions. It is conceivable that further development in the ion trap technology can produce truly ultracold ions in both the vibrational and rotational degrees of freedom, which will further its applications in high-resolution spectroscopy.

ESI allows facile production of free multiply-charged anions and the development of ESI-PES techniques has allowed this class of exotic gaseous species to be characterized spectroscopically for the first time. Intramolecular Coulomb repulsions determine the stability of free multiply-charged anions and result in the repulsive Coulomb barrier. The RCB influences many properties of MCAs and has given rise to novel spectroscopic phenomena. Because of the RCB, threshold detachment is no longer possible for MCAs and the outgoing electron must have sufficient kinetic energies to overcome the RCB. The RCB has made it possible to observe metastable MCAs with negative electron binding energies. Electron tunneling has been observed through the RCB and it has been shown that the nuclear tunneling model is applicable to tunneling in MCAs. Pump-probe experiments have been performed to study the tunneling lifetimes in MCAs and the competition between tunneling and internal conversion. PE imaging has made it possible to directly observe the effects of intramolecular Coulomb repulsion on the electron emission dynamics and it has been found that the electrostatic effects dominate any possible quantum interference effects of the outgoing electron waves in PES of MCAs. Future development by coupling ultracold MCAs and ultrafast lasers should allow more detailed dynamic phenomena to be probed. The combination of ion mobility for isomer separation with PES has shown promise to expand the applications of PES to complex biological MCAs. If cryogenic ion trap technology can be combined with ion

mobility, much better resolved PES is possible, which would be valuable to probe the electrostatic interactions in gaseous biological MCAs.

The development of the third-generation ESI-PES apparatus by coupling a cryogenic Paul trap with high-resolution PE imaging has allowed accurate electronic and vibrational information to be obtained for singly charged anions from ESI and the corresponding neutral species. The use of tunable lasers has made it possible to do resonant two-photon PES for anions state-selectively. Excited dipole-bound states have been observed for a number of cold anions from ESI. The vibrationally cold anions allowed purely vibrational autodetachment spectra to be observed. Resonant PES has been performed by tuning the detachment laser to a specific vibrational level of the dipole-bound state, resulting in highly non-Franck-Condon PE spectra due to the propensity of vibrational autodetachment from the dipole-bound state. It has been shown that the combination of vibrational autodetachment spectroscopy and resonant photoelectron spectroscopy can be a powerful approach to obtain vibrational information for interesting radical species with sufficiently large dipole moments. This technique can even be further developed into conformation-selective PES.[160] Autodetachment from the dipole-bound exited states of anions involves strong vibronic coupling. It would be extremely interesting to conduct pump-probe experiments to probe the autodetachment dynamics and the mechanisms of vibronic coupling.

ACKNOWLEDGMENTS

The development of the first and second generation ESI-PES apparatuses was funded by the Condensed Phase and Interfacial Molecular Science (CPIMS) Program, Chemical Sciences, Geosciences and Biosciences Division of the U.S. Department of Energy, Office of Science, Office of Basic Energy Sciences. The development of the third-generation ESI-PES apparatus was supported by Brown University. The PI was supported previously in part by the CPIMS program to conduct research on multiply-charged anions and their solvent stabilization and by the National Science Foundation, Division of Chemistry to conduct research on the electronic structures of solution-phase species from ESI. I am indebted to many current and previous students and postdoctoral fellows who have contributed to the research discussed in this article. Specifically, I want to thank Professor Chuan-Fan Ding and Dr. Xue-Bin Wang for their contributions to the development of the first-generation ESI-PES, Dr. Xue-Bin Wang and Dr. Hin-Koon Woo for their contributions to the second-generation ESI-PES. I am also grateful to Professor Xiao-Peng Xing, Professor Chuan-Gang Ning, and Dr. Iker León for their contributions to the development of the PE imaging capability and Dr. Hong-Tao Liu for his design and construction of the second-generation cryogenic Paul trap. I would also like to thank Dao-Ling Huang for her assistance in the preparation of several figures.

[1]M. Yamashitat and J. B. Fenn, J. Phys. Chem. **88**, 4451 (1984).
[2]J. B. Fenn, M. Mann, C. K. Meng, S. F. Wong, and C. M. Whitehouse, Science **246**, 64 (1989).
[3]J. B. Fenn, Angew. Chem., Int. Ed. **42**, 3871 (2003).
[4]L. S. Wang, C. F. Ding, X. B. Wang, and J. B. Nicholas, Phys. Rev. Lett. **81**, 2667 (1998).
[5]C. F. Ding, X. B. Wang, and L. S. Wang, J. Phys. Chem. A **102**, 8633 (1998).
[6]X. B. Wang, C. F. Ding, and L. S. Wang, Phys. Rev. Lett. **81**, 3351 (1998).
[7]J. Friedrich, S. Gilb, O. T. Ehrler, A. Behrendt, and M. M. Kappes, J. Chem. Phys. **117**, 2635 (2002).
[8]J. U. Andersen, P. Hvelplund, S. B. Nielsen, S. Tomita, H. Wahlgreen, S. P. Møller, U. V. Pedersen, J. S. Forster, and T. J. D. Jørgensen, Rev. Sci. Instrum. **73**, 1284 (2002).
[9]S. Tomita, J. U. Andersen, E. Bonderup, P. Hvelplund, B. Liu, S. B. Nielsen, U. V. Pedersen, J. Rangama, K. Hansen, and O. Echt, Phys. Rev. Lett. **94**, 053002 (2005).
[10]O. V. Boyarkin, S. R. Mercier, A. Kamariotis, and T. R. Rizzo, J. Am. Chem. Soc. **128**, 2816 (1998).
[11]T. R. Rizzo, J. A. Stearns, and O. V. Boyarkin, Int. Rev. Phys. Chem. **28**, 481 (2009).
[12]J. K. Carr, A. V. Zabuga, S. Roy, T. R. Rizzo, and J. L. Skinner, J. Chem. Phys. **140**, 224111 (2014).
[13]M. F. Bush, J. T. O'Brien, J. S. Prell, R. J. Saykally, and E. R. Williams, J. Am. Chem. Soc. **129**, 1612 (2007).
[14]J. M. F. Bush, R. J. Saykally, and E. R. Williams, J. Am. Chem. Soc. **129**, 2220 (2007).
[15]D. J. Goebbert, T. Wende, R. Bergmann, G. Meijer, and K. R. Asmis, J. Phys. Chem. A **113**, 5874 (2009).
[16]K. R. Asmis and D. M. Neumark, Acc. Chem. Res. **45**, 43 (2012).
[17]C. N. Stedwell, J. F. Galindo, A. E. Roitberg, and N. C. Polfer, Annu. Rev. Anal. Chem. **6**, 267 (2013).
[18]F. O. Talbot, T. Tabarin, R. Antoine, M. Broyer, and P. Dugourd, J. Chem. Phys. **122**, 074310 (2005).
[19]R. Antoine and P. Dugourd, Phys. Chem. Chem. Phys. **13**, 16494 (2011).
[20]M. T. Rodgers, P. B. Armentrout, J. Oomens, and J. D. Steill, J. Phys. Chem. A **112**, 2258 (2008).
[21]Y. W. Nei, N. Hallowita, J. D. Steill, J. Oomens, and M. T. Rodgers, J. Phys. Chem. A **117**, 1319 (2013).
[22]S. Ard, N. Mirsaleh-Kohan, J. D. Steill, J. Oomens, S. B. Nielsen, and R. N. Compton, J. Chem. Phys. **132**, 094301 (2010).
[23]W. E. Boxford and C. E. H. Dessent, Phys. Chem. Chem. Phys. **8**, 5151 (2006).
[24]A. Sen and C. E. H. Dessent, J. Chem. Phys. **141**, 241101 (2014).
[25]J. C. Marcum and J. M. Weber, J. Chem. Phys. **131**, 194309 (2009).
[26]C. S. Byskov, J. M. Weber, and S. B. Nielsen, Phys. Chem. Chem. Phys. **17**, 5561 (2015).
[27]M. Burt, K. Wilson, R. Marta, M. Hasan, W. S. Hopkins, and T. McMahon, Phys. Chem. Chem. Phys. **16**, 24223 (2014).
[28]M. Z. Kamrath, R. A. Relph, T. L. Guasco, C. M. Leavitt, and M. A. Johnson, Int. J. Mass Spectrom. **300**, 91 (2011).
[29]A. B. Wolk, C. M. Leavitt, E. Garand, and M. A. Johnson, Acc. Chem. Res. **47**, 202 (2014).
[30]B. M. Marsh, E. M. Duffy, M. T. Soukup, J. Zhou, and E. Garand, J. Phys. Chem. A **118**, 3906 (2014).
[31]R. A. J. O'Hair and N. J. Rijs, Acc. Chem. Res. **48**, 329 (2015).
[32]L. S. Wang and X. B. Wang, J. Phys. Chem. A **104**, 1978 (2000).
[33]X. B. Wang, X. Yang, and L. S. Wang, Int. Rev. Phys. Chem. **21**, 473 (2002).
[34]T. Waters, X. B. Wang, and L. S. Wang, Coord. Chem. Rev. **251**, 474 (2007).
[35]X. B. Wang and L. S. Wang, Annu. Rev. Phys. Chem. **60**, 105 (2009).
[36]J. R. R. Verlet, D. A. Horkeb, and A. S. Chatterleyc, Phys. Chem. Chem. Phys. **16**, 15043 (2014).
[37]L. S. Wang, C. F. Ding, X. B. Wang, and S. E. Barlow, Rev. Sci. Instrum. **70**, 1957 (1999).
[38]K. Arnold, T. S. Balaban, M. N. Blom, O. T. Ehrler, S. Gilb, O. Hampe, J. E. van Lier, J. M. Weber, and M. M. Kappes, J. Phys. Chem. A **107**, 794 (2003).
[39]O. T. Ehrler, J. M. Weber, F. Furche, and M. M. Kappes, Phys. Rev. Lett. **91**, 113006 (2003).
[40]J. M. Weber, I. N. Ioffe, K. M. Berndt, D. Loffler, J. Friedrich, O. T. Ehrler, A. S. Danell, J. H. Parks, and M. M. Kappes, J. Am. Chem. Soc. **126**, 8585 (2004).
[41]X. B. Wang and L. S. Wang, Rev. Sci. Instrum. **79**, 073108 (2008).
[42]X. B. Wang, H. K. Woo, and L. S. Wang, J. Chem. Phys. **123**, 051106 (2005).
[43]X. B. Wang, H. K. Woo, B. Kiran, and L. S. Wang, J. Phys. Chem. A **109**, 11089 (2005).
[44]T. Waters, H. K. Woo, X. B. Wang, and L. S. Wang, J. Am. Chem. Soc. **128**, 4282 (2006).
[45]X. B. Wang, H. K. Woo, L. S. Wang, B. Minofar, and P. Jungwirth, J. Phys. Chem. A **110**, 5047 (2006).

[46]X. B. Wang, H. K. Woo, B. Kiran, and L. S. Wang, Angew. Chem., Int. Ed. **44**, 4968 (2005).
[47]X. B. Wang, B. Dai, H. K. Woo, and L. S. Wang, Angew. Chem., Int. Ed. **44**, 6022 (2005).
[48]H. K. Woo, X. B. Wang, L. S. Wang, and K. C. Lau, J. Phys. Chem. A **109**, 10633 (2005).
[49]H. K. Woo, X. B. Wang, K. C. Lau, and L. S. Wang, J. Phys. Chem. A **110**, 7801 (2006).
[50]X. B. Wang, J. Yang, and L. S. Wang, J. Phys. Chem. A **112**, 172 (2008).
[51]X. B. Wang, K. Matheis, I. N. Ioffe, A. A. Goryunkov, J. Yang, M. M. Kappes, and L. S. Wang, J. Chem. Phys. **128**, 114307 (2008).
[52]X. B. Wang, X. P. Xing, and L. S. Wang, J. Phys. Chem. A **112**, 13271 (2008).
[53]A. Shokri, J. Schmidt, X. B. Wang, and S. R. Kass, J. Am. Chem. Soc. **134**, 2094 (2012).
[54]H. Wen, G. L. Hou, S. M. Kathmann, M. Valiev, and X. B. Wang, J. Chem. Phys. **138**, 031101 (2013).
[55]S. H. M. Deng, X. Y. Kong, and X. B. Wang, J. Chem. Phys. **142**, 024313 (2015).
[56]I. León, Z. Yang, H. T. Liu, and L. S. Wang, Rev. Sci. Instrum. **85**, 083106 (2014).
[57]I. León, Z. Yang, and L. S. Wang, J. Chem. Phys. **138**, 184304 (2013).
[58]D. Gerlich, Adv. Chem. Phys. **82**, 1 (1992).
[59]Y.-S. Wang, C.-H. Tsai, Y. T. Lee, H.-C. Chang, J. C. Jiang, O. Asvany, S. Schlemmer, and D. Gerlich, J. Phys. Chem. A **107**, 4217 (2003).
[60]S. Trippel, J. Mikosch, R. Berhane, R. Otto, M. Weidemuller, and R. Wester, Phys. Rev. Lett. **97**, 193003 (2006).
[61]O. Asvany, E. Hugo, F. Muller, F. Kuhnemann, S. Schiller, J. Tennyson, and S. Schlemmer, J. Chem. Phys. **127**, 154317 (2007).
[62]P. Jusko, O. Asvany, A.-C. Wallerstein, S. Brunken, and S. Schlemmer, Phys. Rev. Lett. **112**, 253005 (2014).
[63]C. A. Rice, F.-X. Hardy, O. Gause, and J. P. Maier, J. Phys. Chem. Lett. **5**, 942 (2014).
[64]J. G. Redwine, Z. A. Davis, N. L. Burke, R. A. Oglesbee, S. A. McLuckey, and T. S. Zwier, Int. J. Mass Spectrom. **348**, 9 (2013).
[65]A. Fujihara, T. Sato, and S. Hayakawa, Chem. Phys. Lett. **610**, 228 (2014).
[66]K. R. Asmis, M. Brummer, C. Kaposta, G. Santambrogio, G. von Helden, G. Meijer, K. Rademann, and L. Woste, Phys. Chem. Chem. Phys. **4**, 1101 (2002).
[67]C. Hock, M. Schmidt, and B.v. Issendorff, Phys. Rev. B **84**, 113401 (2002).
[68]O. V. Boyarkin and V. Kopysov, Rev. Sci. Instrum. **85**, 033105 (2014).
[69]M. Lange, M. Froese, S. Menk, J. Varju, R. Bastert, K. Blaum, J. R. C. Lopez-Urrutia, F. Fellenberger, M. Grieser, R. von Hahn, O. Heber, K.-U. Kuhnel, F. Laux, D. A. Orlov, M. L. Rappaport, R. Repnow, C. D. Schröter, D. Schwalm, A. Shornikov, T. Sieber, Y. Toker, J. Ullrich, A. Wolf, and D. Zajfman, Rev. Sci. Instrum. **81**, 055105 (2010).
[70]C. J. Johnson, B. B. Shen, B. L. J. Poad, and R. E. Continetti, Rev. Sci. Instrum. **82**, 105105 (2011).
[71]I. Alata, J. Bert, M. Broquier, C. Dedonder, G. Feraud, G. Gregoire, S. Soorkia, E. Marceca, and C. Jouvet, J. Phys. Chem. A **117**, 4420 (2013).
[72]G. Feraud, C. Dedonder-Lardeux, S. Soorkia, and C. Jouvet, J. Chem. Phys. **140**, 024302 (2014).
[73]C. M. Choia, D. H. Choia, N. J. Kima, and J. Heo, Int. J. Mass Spectrom. **314**, 18 (2012).
[74]C. M. Choi, D. H. Choi, J. Heo, N. J. Kim, and S. K. Kim, Angew. Chem., Int. Ed. **51**, 7297 (2012).
[75]S. N. Schauer, P. Williams, and R. N. Compton, Phys. Rev. Lett. **65**, 625 (1990).
[76]J. Kalcher and A. F. Sax, Chem. Rev. **94**, 2291 (1994).
[77]M. K. Scheller, R. N. Compton, and L. S. Cederbaum, Science **270**, 1160 (1995).
[78]A. I. Boldyrev, M. Gutowski, and J. Simons, Acc. Chem. Res. **29**, 497 (1996).
[79]G. R. Freeman and N. H. March, J. Phys. Chem. **100**, 4331 (1996).
[80]A. Dreuw and L. S. Cederbaum, Chem. Rev. **102**, 181 (2002).
[81]X. B. Wang and L. S. Wang, Nature **400**, 245 (1999).
[82]X. B. Wang and L. S. Wang, Phys. Rev. Lett. **83**, 3402 (1999).
[83]X. B. Wang, K. Ferris, and L. S. Wang, J. Phys. Chem. A **104**, 25 (2000).
[84]X. B. Wang, A. P. Sergeeva, X. P. Xing, M. Massaouti, T. Karpuschkin, O. Hampe, A. I. Boldyrev, M. M. Kappes, and L. S. Wang, J. Am. Chem. Soc. **131**, 9836 (2009).
[85]A. Eppink and D. H. Parker, Rev. Sci. Instrum. **68**, 3477 (1997).
[86]E. Surber and A. Sanov, J. Chem. Phys. **116**, 5921 (2002).
[87]A. Osterwalder, M. J. Nee, J. Zhou, and D. M. Neumark, J. Chem. Phys. **121**, 6317 (2004).
[88]X. P. Xing, X. B. Wang, and L. S. Wang, Phys. Rev. Lett. **101**, 083003 (2008).
[89]X. P. Xing, X. B. Wang, and L. S. Wang, J. Chem. Phys. **130**, 074301 (2009).
[90]X. P. Xing, X. B. Wang, and L. S. Wang, J. Phys. Chem. A **114**, 4524 (2010).
[91]X. P. Xing, X. B. Wang, and L. S. Wang, J. Phys. Chem. A **113**, 945 (2009).
[92]C. G. Ning, P. D. Dau, and L. S. Wang, Phys. Rev. Lett. **105**, 263001 (2010).
[93]A. Dreuw and L. S. Cederbaum, Phys. Rev. A **63**, 049904 (2001).
[94]D. A. Horke, A. S. Chatterley, and J. R. R. Verlet, J. Phys. Chem. Lett. **3**, 834 (2012).
[95]D. A. Horke, A. S. Chatterley, and J. R. R. Verlet, J. Chem. Phys. **139**, 084302 (2013).
[96]A. S. Chatterley, D. A. Horke, and J. R. R. Verlet, Phys. Chem. Chem. Phys. **16**, 489 (2014).
[97]X. B. Wang, C. F. Ding, and L. S. Wang, Chem. Phys. Lett. **307**, 391 (1999).
[98]R. N. Compton, A. A. Tuinman, C. E. Klots, M. R. Pederson, and D. C. Patton, Phys. Rev. Lett. **78**, 4367 (1997).
[99]S. Panja, U. Kadhane, J. U. Andersen, A. I. S. Holm, P. Hvelplund, M.-B. S. Kirketerp, S. B. Nielsen, R. N. Compton, J. S. Forster, K. Kilsa, and M. B. Nielsen, J. Chem. Phys. **127**, 124301 (2007).
[100]P. Weis, O. Hampe, S. Gilb, and M. M. Kappes, Chem. Phys. Lett. **321**, 426 (2000).
[101]M. N. Blom, O. Hampe, S. Gilb, P. Weis, and M. M. Kappes, J. Chem. Phys. **115**, 3690 (2001).
[102]D. Löffler, J. M. Weber, and M. M. Kappes, J. Chem. Phys. **123**, 224308 (2005).
[103]O. T. Ehrler, J. P. Yang, A. B. Sugiharto, A. N. Unterreiner, and M. M. Kappes, J. Chem. Phys. **127**, 184301 (2007).
[104]C. Rensing, O. T. Ehrler, J. P. Yang, A.-N. Unterreiner, and M. M. Kappes, J. Chem. Phys. **130**, 234306 (2009).
[105]P. D. Dau, H. T. Liu, J. P. Yang, M.-O. Winghart, T. J. A. Wolf, A.-N. Unterreiner, P. Weis, Y. R. Miao, C. G. Ning, M. M. Kappes, and L. S. Wang, Phys. Rev. A **85**, 064503 (2012).
[106]M.-O. Winghart, J. P. Yang, M. Kühn, A.-N. Unterreiner, T. Wolf, P. D. Dau, H. T. Liu, D. L. Huang, W. Klopper, L. S. Wang, and M. M. Kappes, Phys. Chem. Chem. Phys. **15**, 6726 (2013).
[107]D. A. Horke, A. S. Chatterley, and J. R. R. Verlet, Phys. Rev. Lett. **108**, 083003 (2012).
[108]A. S. Chatterley, D. A. Horke, and J. R. R. Verlet, Phys. Chem. Chem. Phys. **14**, 16155 (2012).
[109]X. Yang, X. B. Wang, E. R. Vorpagel, and L. S. Wang, Proc. Natl. Acad. Sci. U. S. A. **101**, 17588 (2004).
[110]R. Fromherz, G. Gantefor, and A. A. Shvartsburg, Phys. Rev. Lett. **89**, 083001 (2002).
[111]M. Vonderach, O. T. Ehrler, P. Weis, and M. M. Kappes, Anal. Chem. **83**, 1108 (2011).
[112]M. Vonderach, O. T. Ehrler, K. Matheis, T. Karpuschkin, E. Papalazarou, C. Brunet, R. Antoine, P. Weis, O. Hampe, M. M. Kappes, and P. Dugourd, Phys. Chem. Chem. Phys. **13**, 15554 (2011).
[113]M. Vonderach, O. T. Ehrler, K. Matheis, P. Weis, and M. M. Kappes, J. Am. Chem. Soc. **134**, 7830 (2012).
[114]L. Ma, B. von Issendorff, and A. Aguado, J. Chem. Phys. **132**, 104303 (2010).
[115]J. Zhou, E. Garand, and D. M. Neumark, J. Chem. Phys. **127**, 114313 (2007).
[116]J. Zhou, E. Garand, and D. M. Neumark, J. Chem. Phys. **127**, 154320 (2007).
[117]D. M. Neumark, J. Phys. Chem. A **112**, 13287 (2008).
[118]X. B. Wang, C. F. Ding, and L. S. Wang, J. Chem. Phys. **110**, 8217 (1999).
[119]D. L. Huang, P. D. Dau, H. T. Liu, and L. S. Wang, J. Chem. Phys. **140**, 224315 (2014).
[120]K. Stochkel and J. U. Andersen, J. Chem. Phys. **139**, 164304 (2013).
[121]C. Hock, J. B. Kim, M. L. Weichman, T. I. Yacovitch, and D. M. Neumark, J. Chem. Phys. **137**, 244201 (2012).
[122]J. B. Kim, M. L. Weichman, and D. M. Neumark, J. Chem. Phys. **140**, 034307 (2014).
[123]J. B. Kim, M. L. Weichman, and D. M. Neumark, J. Chem. Phys. **141**, 174307 (2014).
[124]M. L. Weichman, J. B. Kim, J. A. DeVine, D. S. Levine, and D. M. Neumark, J. Am. Chem. Soc. **137**, 1420 (2015).
[125]C. G. Ning, X. G. Xiong, Y. L. Wang, J. Li, and L. S. Wang, Phys. Chem. Chem. Phys. **14**, 9323 (2012).
[126]H. T. Liu, Y. L. Wang, X. G. Xiong, P. D. Dau, Z. A. Piazza, D. L. Huang, C. Q. Xu, J. Li, and L. S. Wang, Chem. Sci. **3**, 3286 (2012).
[127]H. T. Liu, D. L. Huang, Y. Liu, L. F. Cheung, P. D. Dau, C. G. Ning, and L. S. Wang, J. Phys. Chem. Lett. **6**, 637 (2015).

[128]H. J. Zhai, C. Bürgel, V. Bonacic-Koutecky, and L. S. Wang, J. Am. Chem. Soc. **130**, 9156 (2008).
[129]R. F. Gunion, M. K. Gilles, M. L. Polak, and W. C. Lineberger, Int. J. Mass Spectrom. Ion Processes **117**, 601 (1992).
[130]A. S. Wightman, Phys. Rev. **77**, 521 (1950).
[131]R. F. Wallis, R. Herman, and H. W. Milnes, J. Mol. Spectrosc. **4**, 51 (1960).
[132]W. R. Garrett, Chem. Phys. Lett. **5**, 393 (1970).
[133]O. H. Crawford, Mol. Phys. **20**, 585 (1971).
[134]C. Desfrancois, B. Baillon, J. P. Schermann, S. T. Arnold, J. H. Hendricks, and K. H. Bowen, Phys. Rev. Lett. **72**, 48 (1994).
[135]J. H. Hendricks, S. A. Lyapustina, H. L. de Clercq, J. T. Snodgrass, and K. H. Bowen, J. Chem. Phys. **104**, 7788 (1996).
[136]C. Desfrancois, V. Periquet, Y. Bouteiller, and J. P. Schermann, J. Phys. Chem. **102**, 1274 (1998).
[137]N. I. Hammer, K. Diri, K. D. Jordan, C. Desfrancois, and R. N. Compton, J. Chem. Phys. **119**, 3650 (2003).
[138]N. I. Hammer, R. J. Hinde, R. N. Compton, K. Diri, K. D. Jordan, D. Radisic, S. T. Stokes, and K. H. Bowen, J. Chem. Phys. **120**, 685 (2004).
[139]A. H. Zimmerman and J. I. Brauman, J. Chem. Phys. **66**, 5823 (1977).
[140]R. L. Jackson, A. H. Zimmerman, and J. I. Brauman, J. Chem. Phys. **71**, 2088 (1979).
[141]R. L. Jackson, P. C. Hiberty, and J. I. Brauman, J. Chem. Phys. **74**, 3705 (1981).
[142]D. A. Walthall, J. M. Karty, B. Ro1mer, O. Ursini, and J. I. Brauman, J. Phys. Chem. A **109**, 8785 (2005).
[143]K. R. Lykke, R. D. Mead, and W. C. Lineberger, Phys. Rev. Lett. **52**, 2221 (1984).
[144]R. D. Mead, K. R. Lykke, W. C. Lineberger, J. Marks, and J. I. Brauman, J. Chem. Phys. **81**, 4883 (1984).
[145]K. R. Lykke, D. M. Neumark, T. Andersen, V. J. Trapa, and W. C. Lineberger, J. Chem. Phys. **87**, 6842 (1987).
[146]J. Marks, J. I. Brauman, R. D. Mead, K. R. Lykke, and W. C. Lineberger, J. Chem. Phys. **88**, 6785 (1988).
[147]K. Yokoyama, G. W. Leach, J. B. Kim, and W. C. Lineberger, J. Chem. Phys. **105**, 10696 (1996).
[148]K. Yokoyama, G. W. Leach, J. B. Kim, W. C. Lineberger, A. I. Boldyrev, and M. Gutowski, J. Chem. Phys. **105**, 10706 (1996).
[149]J. B. Kim, T. I. Yacovitch, C. Hock, and D. M. Neumark, Phys. Chem. Chem. Phys. **13**, 17378 (2011).
[150]H. T. Liu, C. G. Ning, D. L. Huang, P. D. Dau, and L. S. Wang, Angew. Chem., Int. Ed. **52**, 8976 (2013).
[151]J. Simons, J. Am. Chem. Soc. **103**, 3971 (1981).
[152]R. S. Berry, J. Chem. Phys. **45**, 1228 (1966).
[153]H. T. Liu, C. G. Ning, D. L. Huang, and L. S. Wang, Angew. Chem., Int. Ed. **53**, 2464 (2014).
[154]U. Fano, Phys. Rev. **124**, 1866 (1961).
[155]S. T. Edwards, M. A. Johnson, and J. C. Tully, J. Chem. Phys. **136**, 154305 (2012).
[156]C. M. Western, PGOPHER, a program for Simulating Rotational Structure, University of Bristol, 2013, http://pgopher.chm.bris.ac.uk.
[157]D. L. Huang, H. T. Liu, C. G. Ning, G. Z. Zhu, and L. S. Wang, Chem. Sci. **6**, 3129 (2015).
[158]D. L. Huang, G. Z. Zhu, and L. S. Wang, J. Chem. Phys. **142**, 091103 (2015).
[159]D. L. Huang, H. T. Liu, C. G. Ning, and L. S. Wang, J. Chem. Phys. **142**, 124309 (2015).
[160]D. L. Huang, H. T. Liu, C. G. Ning, and L. S. Wang, J. Phys. Chem. Lett. **6**, 2153 (2015).